Journal of Materials Chemistry C

ROYAL SOCIETY OF CHEMISTRY

PAPER

View Article Online
View Journal | View Issue

Cite this: J. Mater. Chem. C, 2022, 10, 13844

Three-dimensional all-inorganic dual halogen emitter $Cs_2Cd_2BrCl_5$ exhibiting broadband white-light emission†

Haiping Xu,‡[a] Xuehua Dong,‡[a] Zhizhuan Zhang,[a] Ling Huang,[b] Hongmei Zeng,[a] Zhien Lin[a] and Guohong Zou*[a]

Received 23rd December 2021,
Accepted 28th January 2022

DOI: 10.1039/d1tc06086d

rsc.li/materials-c

Single-component white-light-emitting materials have received increasing attention due to their excellent luminescence properties. Herein, a novel all-inorganic dual halogen emitter $Cs_2Cd_2BrCl_5$ was successfully synthesized, which features a three-dimensional (3D) network structure. A series of photophysical characterizations show that $Cs_2Cd_2BrCl_5$ exhibits broadband white-light emission at room temperature with a correlated color temperature (CCT) of 4286 K, a color rendering index (CRI) of 84.6 and a high photoluminescence quantum yield (PLQY) of 20.49%. Temperature-dependent emission spectra, structural distortion analysis of the $CdCl_3(Br/Cl)_3$ octahedron, and DFT calculation reveal that the broadband white-light emission of $Cs_2Cd_2BrCl_5$ originates from self-trapped excitons (STEs). Importantly, $Cs_2Cd_2BrCl_5$ shows splendid structural and optical stability, which makes it a potential candidate for light-emitting diodes (LEDs). To our knowledge, it is the first example of white-light emission in 3D Cd-based all-inorganic halide materials, which could provide new insight for the further design and synthesis of all-inorganic single-component white-light emitters.

[a] College of Chemistry, Sichuan University, Chengdu, 610064, P. R. China. E-mail: zough@scu.edu.cn
[b] College of Chemistry and Materials Science, Sichuan Normal University, Chengdu 610066, P. R. China

† Electronic supplementary information (ESI) available: Additional crystallographic data, EDS, CIE chromaticity coordinates, and time-resolved decay curves. CCDC 2129940. For ESI and crystallographic data in CIF or other electronic format see DOI: 10.1039/d1tc06086d

‡ These authors contributed equally to this work.

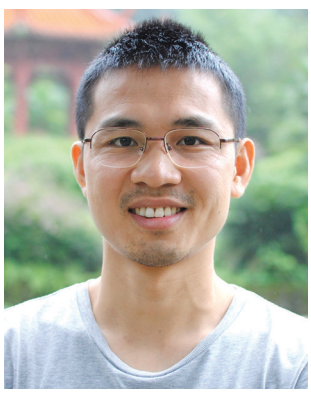

Guohong Zou

Professor Guohong Zou earned B.S. degree from Central South University in 2008, and got his PhD degree in 2013 from Fujian Institute of Research on the Structure of Matter, Chinese Academy of Sciences, China, under the direction of Professor Ning Ye on discovering new nonlinear optical materials. He performed postdoctoral research in the group of Prof. Kang Min Ok at Chung-Ang University, Keroa, on the UV nonlinear optical crystals. Currently, he is a Professor at Sichuan University. His research includes discovering novel inorganic optical materials.

Introduction

In the past few years, solid-state lighting technology (SSL) has greatly affected our lives due to its application in light-emitting diodes (LEDs), sensors and displays.[1–8] Achieving white-light emission is considered a key step in the effective use of SSL. Generally, there are three ways to achieve white-light emission: one is *via* a three-component emitter with a mixture of red, blue, and green light sources;[9–11] another is *via* a two-component emitter that combines yellow and blue light sources; and the third is *via* single-component white-light-emitting materials. Multi-component white-light-emitting materials have a high quantum efficiency and excellent color rendering properties. However, the serious re-absorption between the multiple components and the discontinuity of the emission spectrum in the visible range hinder their application.[12,13] By contrast, single-component white-light-emitting materials overcome the above disadvantages, and have attracted increasing attention due to their simple preparation process, lower cost, and good color rendering.[14,15]

Single-component white-light emission has made remarkable achievements in organic molecules, inorganic nanocrystals and metal–organic frameworks.[16,17] These materials exhibit excellent optical properties, but their synthesis involves complicated processing.[18] Recently, organic–inorganic hybrid halide-based white-light-emitting materials have received

extensive attention due to their high color purity and adjustable structural dimensions. For example, Kanatzidis *et al.* reported a series of lead bromide perovskites including α-(DMEN)$PbBr_4$, (DMAPA)$PbBr_4$ and (DMABA)$PbBr_4$. They possess a 2D layered structure and exhibit inherent white-light emission.[19] In addition, Karundasa *et al.* synthesized (EDBE)[PbX_4] (X = Cl, Br, I) perovskites, which also exhibit broadband white-light emission.[20] The broadband emissions of such compounds are ascribed to self-trapped excitons (STEs), which are caused by strong electron–phonon coupling in the distorted structure. In addition to Pb-based halide white-light-emitting materials, some Cd-based organic–inorganic hybrid halide white-light emitters have also been reported recently, including (2cepiH)$CdCl_3$ and $(C_6H_{11}NH_3)_2CdBr_4$, which possess one-dimensional (1D) chain and two-dimensional (2D) layered structures, respectively, and all of them exhibit white-light emission.[21,22] Compared with organic–inorganic hybrid halide white-light-emitting materials, all-inorganic halide emitters may have more research value due to their relatively excellent thermal stability. At present, reports on Cd-based all-inorganic halide white-light-emitting materials are very limited. Although Luo *et al.* reported the white-light emitter $Rb_2CdCl_2I_2$, it possesses a 2D layered structure.[23] 3D Cd-based all-inorganic white-light halide materials have not been reported so far.

In this work, we reported a new 3D all-inorganic dual halogen emitter $Cs_2Cd_2BrCl_5$, which exhibits broadband white-light emission at room temperature. The white-light emission of $Cs_2Cd_2BrCl_5$ is attributed to STEs as revealed by the analysis of octahedral structure distortion, temperature-dependent emission spectra and DFT theoretical calculations. Moreover, $Cs_2Cd_2BrCl_5$ possesses good structural thermal stability and an excellent optical performance compared with the organic–inorganic hybrid materials. As far as we know, this emitter is the first example of white-light emission in Cd-based 3D all-inorganic halides. Our studies not only enrich the research on Cd-based light-emitting materials but also provide insight into the design and synthesis of all-inorganic dual-halogen white-light emitters.

Experimental section

Synthesis

Analytical grade reagents including $CdBr_2{\cdot}4H_2O$ (AR, 98%) and CsCl (AR, 99%) were used directly without further purification. The $Cs_2Cd_2BrCl_5$ single crystals were synthesized *via* a hydrothermal method from the reactions of a mixture of $CdBr_2{\cdot}4H_2O$ (0.344 g, 1 mmol) and CsCl (0.337 g, 2 mmol) dissolved in 3 mL deionized water. The mixture was sealed into a 23 mL Teflon autoclave and heated at 180 °C for 3 days before cooling to room temperature. The target product was washed with alcohol and then dried in an oven at 40 °C. Transparent colorless rod crystals were obtained.

Characterization

Single-crystal X-ray diffraction was measured at 293.6(8) K using a Rigaku XtaLAB Synergy R diffractometer with graphite monochromatic Cu Kα (λ = 1.54184 Å) radiation (Table 1). Powder X-ray diffraction (XRD) data were obtained using a Rigaku D/MAX-rA diffractometer with Cu-Kα radiation (λ = 1.5418 Å). Thermogravimetric (TG) analyses were recorded in a flow of N_2 with a heating rate of 10 °C min^{-1} using a Netzsch STA 449c analyzer. Scanning electron microscope (SEM)/energy-dispersive (EDS) analyses were performed using a Hitachi S-3400N/Horiba Energy EX-250 instruments. The UV-vis absorption spectra were obtained at room temperature using a PerkinElmer Lambda-950 UV/VIS spectrophotometer. The band structure, density of states (DOS)/partial density of states (PDOS), and electron density difference (EDD) diagrams were calculated through first principles. Gradient correction functional (GGA) and Perdew–Burke–Ernzerhof (PBE) were used for all calculations. The excitation spectra, emission spectra and photoluminescence quantum yield (PLQY) were measured using an Edinburgh FS-5 fluorescence spectrometer with a calibrated integrating sphere system. The temperature-dependent emission spectra and time-resolved PL decay curves were measured using a Fluoromax-3 fluorescence spectrometer.

Table 1 Crystal data and structure refinement for $Cs_2Cd_2BrCl_5$

Formula	$Cs_2Cd_2BrCl_5$
Formula weight	747.80
Crystal system	Hexagonal
Space group	$P6_3/mmc$
a (Å)	7.4571(2)
b (Å)	7.4571(2)
c (Å)	12.5222(6)
V (Å^3)	603.05(4)
Z	2
D_{calcd} (g cm^{-3})	4.118
Temperature (K)	293(2)
λ (Å)	0.71073
F (000)	652.0
μ (mm^{-1})	13.833
GOF on F^2	1.267
R_1, wR_2 ($I > 2\sigma(I)$)[a]	0.0285/0.0758

[a] $R_1(F) = \sum||F_o| - |F_c||/\sum|F_o|$; $wR_2(F_o^2) = [\sum w(F_o^2 - F_c^2)^2/\sum w(F_o^2)^2]^{1/2}$.

Result and discussions

Crystal structure, octahedral distortion, phase purity and thermal analysis

Single-crystal X-ray diffraction (SCXRD) analysis demonstrates that $Cs_2Cd_2BrCl_5$ crystallizes in the hexagonal space group of $P6_3/mmc$ (no. 194). There are one independent Cd atom, one Cl atom, one Br/Cl co-occupation atom and two Cs atoms in the crystallographic asymmetric unit of $Cs_2Cd_2BrCl_5$. The Cd atom is coordinated with three Cl atoms and three co-occupied Br/Cl atoms forming a $CdCl_3(Br/Cl)_3$ octahedron. Two $CdCl_3(Br/Cl)_3$ octahedra are connected forming a $Cd_2Cl_6(Br/Cl)_3$ dimer *via* sharing of the three co-occupied Br/Cl atoms (Fig. 1a). The Cd–Cl and Cd–Br bond lengths range from 2.604 to 2.691 Å (Fig. 1a). The adjacent $Cd_2Cl_6(Br/Cl)_3$ dimers are inter-linked, forming a 2D layer *via* sharing Cl atoms along the *ac* plane (Fig. 1b), and this corrugated 2D layer is further linked *via* sharing Cl atoms along the *b* axis, resulting in the 3D structure

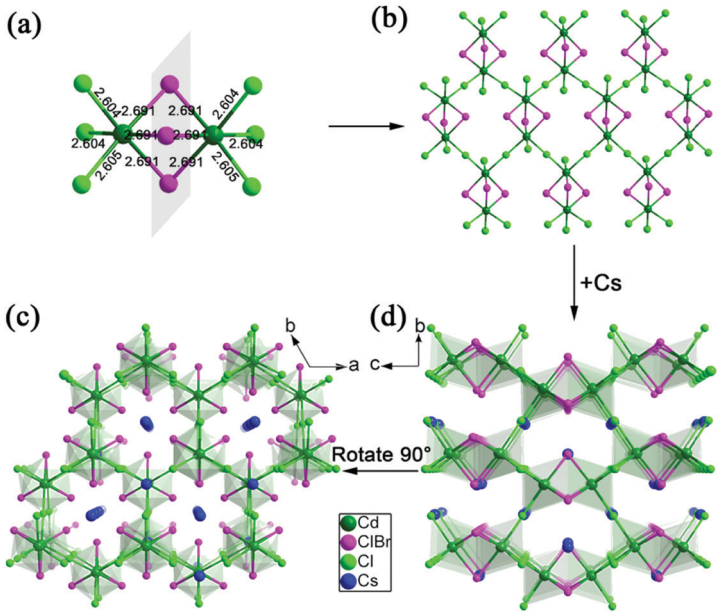

Fig. 1 (a) Coordination of $Cd_2Cl_6(Br/Cl)_3$ dimers and their bond lengths; (b) 2D layer structure built from adjacent $Cd_2Cl_6(Br/Cl)_3$ dimers that are interlinked by sharing the Cl atoms along the *ac* plane; (c) crystal structure of $Cs_2Cd_2BrCl_5$ viewed along the *ab* plane; and (d) crystal structure of $Cs_2Cd_2BrCl_5$ viewed along the *bc* plane.

(Fig. 1c and d). The Cs ions are regularly inserted in the 3D anion framework along the *c* axis and play a role in maintaining the charge balance (Fig. 1c and d). It is worth noting that the Cd–Cl bond lengths are shorter than those of the co-occupied Cd–Br/Cl bonds, which indicates the $CdCl_3(Br/Cl)_3$ octahedron is distorted. The distortion degree of the $CdCl_3(Br/Cl)_3$ octahedron can be evaluated using the following formula:[24,25]

$$\Delta d = \frac{1}{6}\sum_{n=1}^{6}[(d_n - d)/d]^2$$

where d_n represents the length of six independent Cd–Cl or Cd–Br/Cl bonds, and d is their average bond length. The value of Δd is calculated as 2.68×10^{-4}, which is comparable to the reported lead-based halide materials of $(BA)_2PbI_4$ ($\Delta d = 3.5 \times 10^{-4}$), ((DMAPA)$PbBr_4$) ($\Delta d = 1.1 \times 10^{-4}$) and (DMABA)$PbBr_4$ ($\Delta d = 4.3 \times 10^{-4}$), indicating that the $CdCl_3(Br/Cl)_3$ octahedron shows structural distortion.[17,26] The distortion of the Cd–Cl/Br framework facilitates the formation of STEs, resulting in broadband emission. The powder XRD data of $Cs_2Cd_2BrCl_5$ were measured to verify the phase purity, and the results showed that the experimental data are in accordance with the calculated XRD pattern (Fig. 2a). In addition, EDS analysis of $Cs_2Cd_2BrCl_5$ showed that the elemental content matches well with the theoretical values (Fig. S1, ESI†). Moreover, the TGA and DSC curves of $Cs_2Cd_2BrCl_5$ were collected at a heating rate of 10 °C min^{-1} in the temperature range from RT to 850 °C (Fig. 2b). The TGA curve shows that there is almost no heat loss until the heating temperature exceeds 500 °C, and that $Cs_2Cd_2BrCl_5$ did not undergo any phase change before decomposition can be seen in the DSC curve. The above results indicate that $Cs_2Cd_2BrCl_5$ has a high thermal stability and is an ideal candidate for single-component white-light-emitting materials in SSL applications.

PL properties and optical stability analysis

The photoluminescence (PL) properties of $Cs_2Cd_2BrCl_5$ at room temperature were fully explored. Fig. 3a shows that the

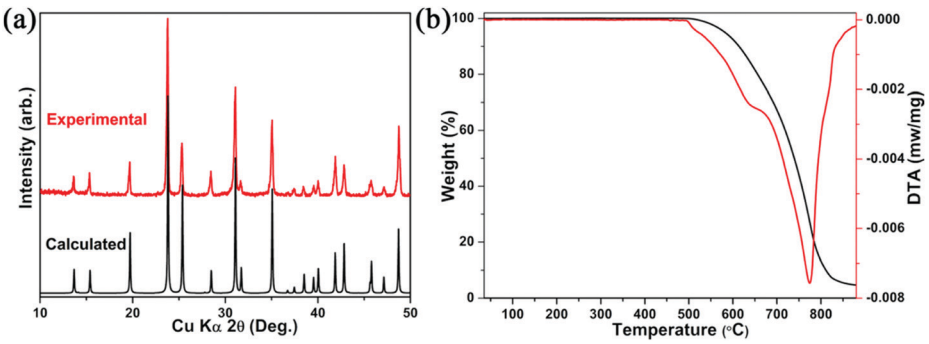

Fig. 2 (a) XRD pattern of $Cs_2Cd_2BrCl_5$ obtained *via* a hydrothermal method, and (b) TG–DSC curves of $Cs_2Cd_2BrCl_5$.

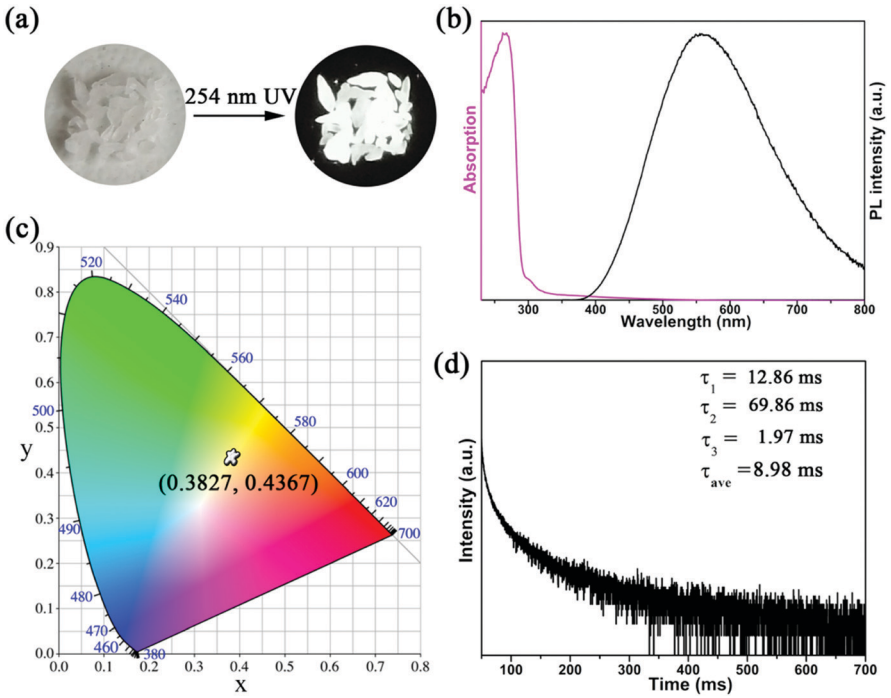

Fig. 3 PL properties of compound $Cs_2Cd_2BrCl_5$ at room temperature: (a) images of $Cs_2Cd_2BrCl_5$ crystals under ambient light and 254 nm UV-light excitation, (b) UV-vis absorption spectrum (purple line) and emission spectrum (black line), (c) CIE chromaticity coordinates, and (d) lifetime decay curve.

$Cs_2Cd_2BrCl_5$ bulk crystals are colorless and transparent under ambient light and emit bright white light upon 254 nm UV-light irradiation. As shown in the purple line of Fig. 3b, the absorption edge of 291 nm was observed and the corresponding experimental band gap is 4.25 eV. Upon 285 nm excitation, $Cs_2Cd_2BrCl_5$ exhibits broadband emission covering the entire visible-light range with the strongest emission peak at 557 nm and a FWHM of 206 nm (the black line of Fig. 3b). The large Stokes shift of 272 nm is attributed to the strong electron–phonon coupling in the distorted $CdCl_3(Br/Cl)_3$ octahedron.[27] As illustrated in Fig. 3c, the CIE chromaticity coordinates of $Cs_2Cd_2BrCl_5$ are (0.3827, 0.4367) and the correlated color temperature (CCT) is 4286 K, which corresponds to white-light emission. In addition, the CRI reaches up to 84.6, which is higher than most commercial light-emitting diodes (with a CRI of 80), making it a candidate for advanced color-critical applications. Moreover, the PLQY of $Cs_2Cd_2BrCl_5$ was measured to be 20.49%, which is relatively high for single-component white-light-emitting materials, whose PLQY values are usually <10%. For example, the PLQY values of $(C_5H_9NH_3)_4CdBr_4$, $(2meptH_2)_4PbCl_4$ and $(EDBE)_4PbBr_4$ are 1%, 1.05% and 9%, respectively.[28–30] The time-resolved PL decay curve shows that the average lifetime of $Cs_2Cd_2BrCl_5$ is 8.98 ms, which was obtained *via* triple-exponential fitting (Fig. 3d). As previously reported, the emission of many semiconductor materials originates from surface defects, and the emission will be quenched as the particles aggregate.[31–33] Therefore, the emission spectra of bulk crystals and ground powder samples were measured to determine the emission origin. Fig. 4a reflects that there is no difference in the emission spectra of bulk crystals and ground powder, suggesting that the emission of $Cs_2Cd_2BrCl_5$ is not caused by surface defects but is inherent emission. Considering the large Stokes shift and wide FWHM, we speculate that the white-light emission of $Cs_2Cd_2BrCl_5$ can be ascribed to STEs.[34–37] Generally considered, halide luminescent materials exhibit poor structural and photophysical stability. Therefore, the emission spectra of fresh crystals, bulk crystals placed in the air for 120 d and after irradiation for 12 h with 254 nm UV light (300 W cm^{-2} Xe lamp) were collected. As shown in Fig. 4b, the emission spectra present similar profiles, and the emission intensities of the crystals after treatment are only slightly lower than that of the fresh crystals, indicating that $Cs_2Cd_2BrCl_5$ shows excellent structural and photophysical stability.

Mechanism study *via* temperature-dependent PL spectra

To explore the thermal quenching behavior and emission mechanism of compound $Cs_2Cd_2BrCl_5$, we collected the temperature-dependent PL spectra from 287 to 77 K at identical intervals of 30 K. As shown in Fig. 5a, it can be observed that as the temperature decreases, the intensity of the emission peak is gradually enhanced. The above phenomenon can be explained as lowering the temperature helps to reduce the non-radiative transitions, resulting in more energy being presented in the form of light rather than thermal loss. The activation energy (ΔE_a) of $Cs_2Cd_2BrCl_5$ for thermal quenching can be expressed clearly using the Arrhenius equation:[38–41]

$$I_T = \frac{I_0}{1 + c \times \exp\left(-\frac{\Delta E}{kT}\right)}$$

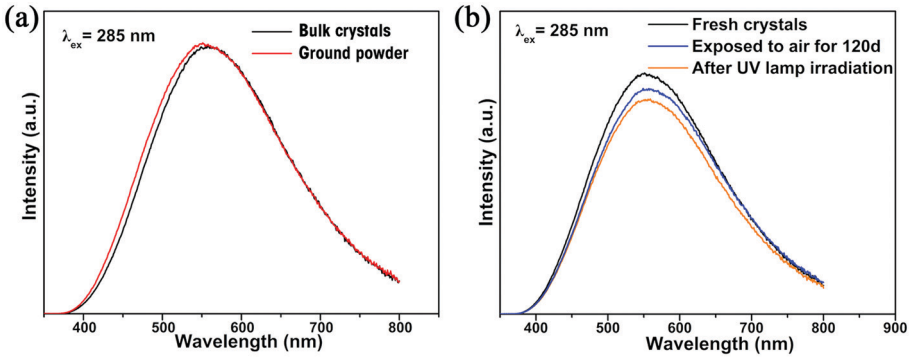

Fig. 4 (a) PL spectra of bulk crystals and ground powder for $Cs_2Cd_2BrCl_5$, and (b) emission spectra of fresh $Cs_2Cd_2BrCl_5$ crystals, crystals exposed to air for 120 d, and after 12 h of UV-lamp irradiation.

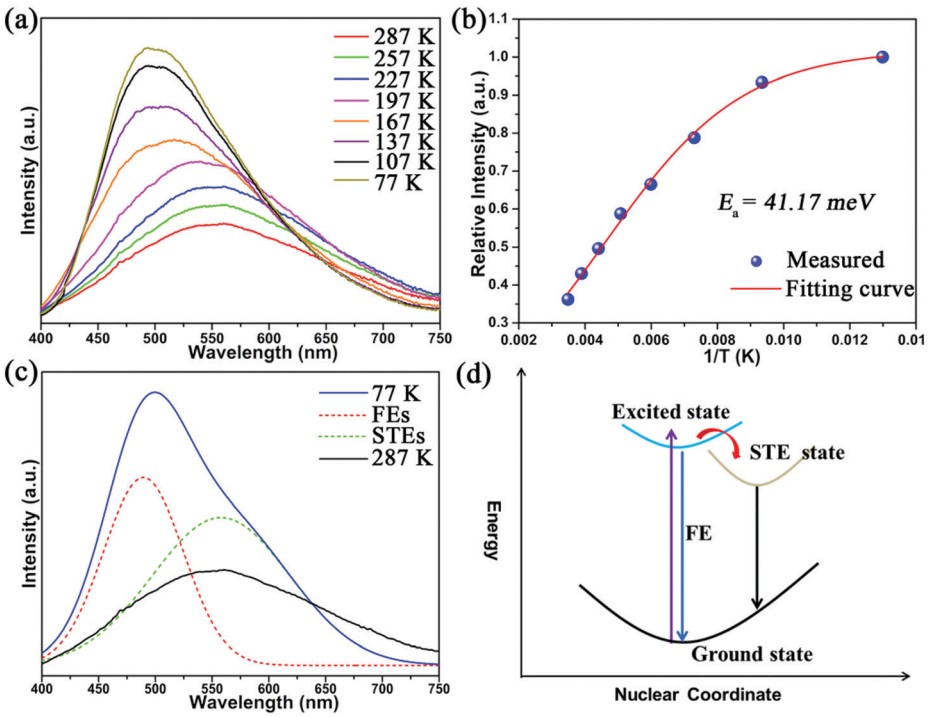

Fig. 5 (a) Temperature-dependent emission spectra; (b) functional relationship between 1/*T* and the integrated PL intensity; (c) emission spectrum at 77 K (solid blue line) and 287 K (solid black line), with the emission spectra of FEs (red dashed line) and STEs (green dashed line) obtained *via* Gaussian fitting to split the emission spectrum at 77 K; and (d) corresponding emission mechanism configuration diagram of $Cs_2Cd_2BrCl_5$.

where I_0 and I_T represent the PL intensity at the initial temperature and the test temperature T, respectively. The parameters c and ΔE_a represent the frequency factor and activation energy, respectively, k is the Boltzmann constant (8.617×10^{-5} eV K^{-1}), and the fitting result is displayed in Fig. 5b. The activation energy (ΔE_a) of $Cs_2Cd_2BrCl_5$ is fitted as 41.17 meV, which is equivalent to previously reported halide luminescent materials.[42,43] In particular, the emission spectra of $Cs_2Cd_2BrCl_5$ at 287 K and 77 K are revealed in Fig. 5c. It can be clearly seen that when the test temperature is reduced from 287 K to 77 K, in addition to the broadband emission at room temperature, a high-energy narrowband emission at 480 nm appears. The corresponding CIE chromaticity coordinates changes from (0.3827, 0.4367) for white light to (0.2807, 0.3926) for green light (Fig. S2, ESI†). Moreover, the time-resolved decay curve of $Cs_2Cd_2BrCl_5$ at 77 K was also measured (Fig. S3, ESI†). Under excitation at 285 nm, with monitoring at 480 nm, the lifetime is 2.2 ns, and while monitoring at 557 nm, the lifetime is 9.13 ms.

We attribute the narrowband emission at 480 nm to the emission of free excitons (FEs), while the broadband emission at 557 nm can be ascribed to the emission of self-trapped excitons (STEs).[44,45] The FE and STE emission can be well represented using Gaussian fitting to split the emission

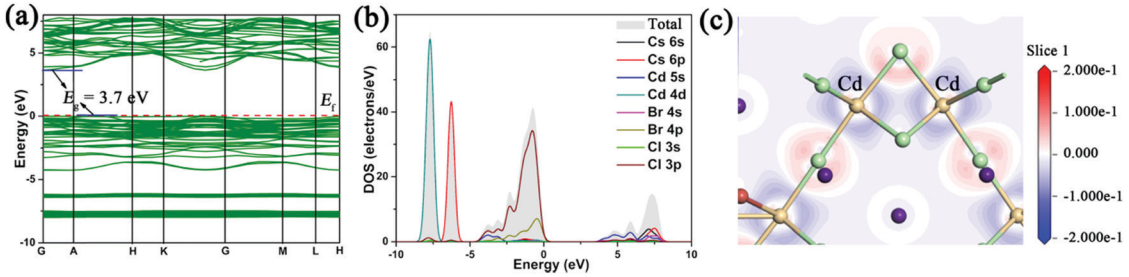

Fig. 6 (a) $Cs_2Cd_2BrCl_5$ band structure; (b) TDOS and PDOS, where the Fermi level (E_f) is normalized to 0 eV; and (c) EDD map for $Cs_2Cd_2BrCl_5$.

spectrum at 77 K (green and red dashed lines in Fig. 5c). Moreover, the emission mechanism of $Cs_2Cd_2BrCl_5$ can be further explained using a configuration diagram (Fig. 5d).[46,47] Under UV-light excitation, the electrons in the ground state are first excited to the FE excited state, and then they transit to the STE excited state through the relaxation process. Finally, the excitons return to the ground state from the STE excited state. The STEs dominate at high temperature (287 K) because there is sufficient energy to overcome the energy barrier from FEs to STEs, resulting in a strong broadband emission. However, when the temperature drops to 77 K, the thermal energy is not sufficient to overcome the barrier between the two energy levels, meaning that only a small proportion of the excitons can cross the barrier to enter the STE excited state, and most of them directly return to the ground state from the FE excited state. Therefore, in addition to the broadband emission, a strong high-energy narrowband emission peak also appears at 77 K, and the intensity of the narrowband emission is stronger than that of broadband emission.

Electronic structure calculations

In order to evaluate the electronic structure and further confirm the PL mechanism of $Cs_2Cd_2BrCl_5$, the band structure, partial density of states and electron-density difference map were calculated using the first principles density functional theory method. As shown in Fig. 6a, the conduction band minimum (CBM) and the valence band maximum (VBM) lie at different locations (in the areas of GA and AH, respectively), indicating that $Cs_2Cd_2BrCl_5$ is an indirect band gap compound. The calculated band gap is 3.7 eV, which is smaller than experimental band gap (4.25 eV). As is well known, DFT–GGA methods will bring down the conduction band levels and therefore underestimate the calculated band gap.[48–51] The total densities of states (TDOS) and partial densities of states (PDOS) of $Cs_2Cd_2BrCl_5$ are calculated and plotted in Fig. 6b. It can be seen that the top of the valence band and the bottom of the conduction band are mainly composed of Cl-3p, Br-4p and Cd-5s orbitals, indicating that there are relatively strong bonds between Cd and Cl, and between Cd and Br. Since the optical properties of materials are mainly determined by the state near the forbidden band, the photoluminescence of $Cs_2Cd_2BrCl_5$ is contributed by the $CdCl_3(Br/Cl)_3$ octahedra. The electron density difference (EDD) map (Fig. 6c) shows that the electron cloud of Cd atoms has significant steric activity and the $CdCl_3(Br/Cl)_3$ octahedra are distorted. The distorted structure facilitates electron–phonon coupling to form STEs, resulting in broadband emission.

Conclusions

In summary, the 3D all-inorganic dual halogen emitter $Cs_2Cd_2BrCl_5$ was obtained through a hydrothermal method. $Cs_2Cd_2BrCl_5$ exhibits broadband white-light emission at room temperature with a CCT of 4286 K, a CRI of 84.6 and a high PLQY of 20.49%. In addition, $Cs_2Cd_2BrCl_5$ possesses excellent structural and thermal stability, indicating that $Cs_2Cd_2BrCl_5$ is a promising single-component white-light-emitting material. Photophysical studies show that the broadband emission of $Cs_2Cd_2BrCl_5$ is attributed to the emission of STEs that originate from the strong electron–phonon coupling in the octahedral distortion, which was further confirmed *via* DFT calculations. Our studies will provide new insight for the further exploration of novel all-inorganic white-light emitters.

Conflicts of interest

There are no conflicts to declare.

Acknowledgements

This work was supported by the National Natural Science Foundation of China (no. 21875146, 22071158, and 22122106).

Notes and references

1 C. K. Zhou, Y. Tian, Z. Yuan, H. R. Lin, B. H. Chen, R. J. Clark, T. Dilbeck, Y. Zhou, J. Hurley, J. Neu, T. Besara, T. Siegrist, P. I. Djurovich and B. W. Ma, *ACS Appl. Mater. Interfaces*, 2017, **9**, 44579–44583.
2 X. Y. Huang, Qi Sun and B. Devakumar, *Mater. Today Chem.*, 2020, **17**, 100288.
3 M. D. Smith, B. A. Connor and H. I. Karunadasa, *Chem. Rev.*, 2019, **119**, 3104–3139.
4 S. Reineke, F. Lindner, G. Schwartz, N. Seidler, K. Walzer, B. Lüssem and K. Leo, *Nature*, 2009, **459**, 234–238.
5 W. Ki and J. Li, *J. Am. Chem. Soc.*, 2008, **130**, 8114–8115.

6 M. S. Wang, S. P. Guo, Y. Li, L. Z. Cai, J. P. Zou, G. Xu, W. W. Zhou, F. K. Zheng and G. C. Guo, *J. Am. Chem. Soc.*, 2009, **131**, 13572–13573.
7 X. D. Wang, O. S. Wolfbeis and R. J. Meier, *Chem. Soc. Rev.*, 2013, **42**, 7834.
8 Y. L. Deng, L. Huang, X. H. Dong, L. Wang, K. M. Ok, H. M. Zeng, Z. E. Lin and G. H. Zou, *Angew. Chem., Int. Ed.*, 2020, **59**, 21151–21156.
9 X. Bai, G. Caputo, Z. D. Hao, V. T. Freitas, J. H. Zhang, R. L. Longo, O. L. Malta, R. A. S. Ferreira and N. Pinna, *Nat. Commun.*, 2014, **5**, 5702.
10 Y. Q. Li, A. Rizzo, R. Cingolani and G. Gigli, *Adv. Mater.*, 2006, **18**, 2545–2548.
11 W. B. Im, N. George, J. Kurzman, S. Brinkley, A. Mikhailovsky, J. Hu, B. F. Chmelka, S. P. DenBaars and R. Seshadri, *Adv. Mater.*, 2011, **23**, 2300–2305.
12 M. J. Bowers, J. R. McBride and S. J. Rosenthal, *J. Am. Chem. Soc.*, 2005, **127**, 15378–15379.
13 Z. W. Zhuang, C. D. Peng, G. Y. Zhang, H. M. Yang, J. L. Yin and H. H. Fei, *Angew. Chem., Int. Ed.*, 2017, **56**, 14411–14416.
14 Y. Liu, M. Nishiura, Y. Wang and Z. M. Hou, *J. Am. Chem. Soc.*, 2006, **128**, 5592–5593.
15 G. M. Song, M. Z. Li, S. Z. Zhang, N. Z. Wang, P. F. Gong, Z. G. Xia and Z. S. Lin, *Adv. Funct. Mater.*, 2020, **30**, 2002468.
16 J. R. McBride, A. D. Dukes, M. A. Schreuder and S. J. Rosenthal, *Chem. Phys. Lett.*, 2010, **498**, 1–9.
17 S. K. Panda, S. G. Hickey, H. V. Demir and A. Eychmller, *Angew. Chem., Int. Ed.*, 2011, **50**, 4432–4436.
18 V. Bachmann, C. Ronda and A. Meijerink, *Chem. Mater.*, 2009, **21**, 2077–2084.
19 L. L. Mao, Y. L. Wu, C. C. Stoumpos, M. R. Wasielewski and M. G. Kanatzidis, *J. Am. Chem. Soc.*, 2017, **139**, 5210–5215.
20 E. R. Dohner, A. Jaffe, L. R. Bradshaw and H. I. Karunadasa, *J. Am. Chem. Soc.*, 2014, **136**, 13154–13157.
21 Z. K. Qi, Y. L. Chen, Y. Guo, X. L. Yang, F. Q. Zhang, G. J. Zhou and X. M. Zhang, *J. Mater. Chem. C*, 2021, **9**, 88–94.
22 A. Yangui, S. Pillet, E. E. Bendeif, A. Lusson, S. Triki, Y. Abid and K. Boukheddaden, *ACS Photonics*, 2018, **5**, 1599–1611.
23 X. F. Li, S. S. Wang, S. G. Zhao, L. N. Li, Y. Q. Li, B. Q. Zhao, Y. G. Shen, Z. Y. Wu, P. Shan and J. H. Luo, *Chem. – Eur. J.*, 2018, **24**, 9243–9246.
24 C. Sun, Y. D. Yue, W. F. Zhang, X. Y. Sun, Y. Du, H. M. Pan, Y. Y. Ma, Y. C. He, M. T. Li and Z. H. Jing, *CrystEngComm*, 2020, **22**, 1480–1486.
25 G. J. Zhou, X. X. Jiang, M. Molokeev, Z. S. Lin, J. Zhao, J. Wang and Z. G. Xia, *Chem. Mater.*, 2019, **31**, 5788–5795.
26 C. C. Stoumpos, D. H. Cao, D. J. Clark, J. Young, J. M. Rondinelli, J. I. Jang, J. T. Hupp and M. G. Kanatzidis, *Chem. Mater.*, 2016, **28**, 2852–2867.
27 Y. Y. Jing, Y. Liu, M. Z. Li and Z. G. Xia, *Adv. Opt. Mater.*, 2021, **9**, 2002213.
28 S. S. Wang, L. N. Li, Z. H. Sun, C. M. Ji, S. J. Liu, Z. Y. Wu, S. G. Zhao, M. C. Hong and J. H. Luo, *J. Mater. Chem. C*, 2017, **5**, 4731–4735.
29 S. S. Wang, Y. P. Yao, Z. Y. Wu, Y. Peng, L. N. Li and J. H. Luo, *J. Mater. Chem. C*, 2018, **6**, 12267–12272.
30 E. R. Dohner, A. Jaffe, L. R. Bradshaw and H. I. Karunadasa, *J. Am. Chem. Soc.*, 2014, **136**, 13154–13157.
31 M. Noh, T. Kim, H. Lee, C. K. Kim, S. W. Joo and K. Lee, *Colloids Surf., A*, 2010, **359**, 39–44.
32 T. E. Rosson, S. M. Claiborne, J. R. McBride, B. S. Stratton and S. J. Rosenthal, *J. Am. Chem. Soc.*, 2012, **134**, 8006–8009.
33 Z. Y. Wu, C. Ji, Z. H. Sun, S. S. Wang, S. G. Zhao, W. C. Zhang, L. N. Li and J. H. Luo, *J. Mater. Chem. C*, 2018, **6**, 1171–1175.
34 Y. W. Ge, Q. Wang, F. Yang, L. Huang, D. J. Gao, J. Bi and G. H. Zou, *Inorg. Chem.*, 2021, **60**, 8322–8330.
35 J. L. Huang, B. B. Su, E. H. Song, M. S. Molokeev and Z. G. Xia, *Chem. Mater.*, 2021, **33**, 4382–4389.
36 Y. Zhou, Z. J. Yong, K. C. Zhang, B. M. Liu, Z. W. Wang, J. S. Hou, Y. Z. Fang, Y. Zhou, H. T. Sun and B. Song, *J. Phys. Chem. Lett.*, 2016, **7**, 2735–2741.
37 M. Z. Li, Y. W. Li, M. S. Molokeev, J. Zhao, G. R. Na, L. J. Zhang and Z. G. Xia, *Adv. Opt. Mater.*, 2020, **8**, 2000418.
38 G. J. Zhou, Z. Y. Liu, M. S. Molokeev, Z. W. Xiao, Z. G. Xia and X. M. Zhang, *J. Mater. Chem. C*, 2021, **9**, 2047–2053.
39 F. Hong, H. M. Cheng, G. X. Liu, X. T. Dong, W. S. Yu and J. X. Wang, *Inorg. Chem.*, 2018, **57**, 9892–9901.
40 F. Hong, H. P. Xu, L. Yang, G. X. Liu, C. Song, X. T. Dong and W. S. Yu, *New J. Chem.*, 2019, **43**, 14859–14871.
41 F. Hong, G. Pang, L. J. Diao, Z. D. Fu, G. X. Liu, X. T. Dong, W. S. Yu and J. X. Wang, *Dalton Trans.*, 2020, **49**, 13805–13817.
42 C. Sun, W. L. He, M. J. Liu, W. J. Pan, L. F. Dong, G. Chen, G. D. Liu and X. W. Lei, *Chem. – Asian J.*, 2020, **15**, 3050–3058.
43 C. Y. Yue, C. Sun, D. Y. Li, Y. H. Dong, C. L. Wang, H. F. Zhao, H. Jiang, Z. H. Jing and X. W. Lei, *Inorg. Chem.*, 2019, **58**, 10304–10312.
44 X. T. Li, P. J. Guo, M. Kepenekian, I. Hadar, C. Katan, J. Even, C. C. Stoumpos, R. D. Schaller and M. G. Kanatzidis, *Chem. Mater.*, 2019, **31**, 3582–3590.
45 C. Sun, Y. H. Guo, S. S. Han, J. Z. Li, K. Jiang, L. F. Dong, Q. L. Liu, C. Y. Yue and X. W. Lei, *Angew. Chem., Int. Ed.*, 2020, **59**, 16465–16469.
46 J. H. Wei, J. F. Liao, X. D. Wang, L. Zhou, Y. Jiang and D. B. Kuang, *Matter*, 2020, **3**, 892–903.
47 L. Zhou, J. F. Liao, Z. G. Huang, J. H. Wei, X. D. Wang, H. Y. Chen and D. B. Kuang, *Angew. Chem., Int. Ed.*, 2019, **58**, 15435–15440.
48 Q. Jing, X. Y. Dong, X. L. Chen, Z. H. Yang, S. L. Pan and C. Lei, *Chem. Phys.*, 2015, **453**, 42–46.
49 A. J. Cohen, P. Mori-Sánchez and W. T. Yang, *Phys. Rev. B: Condens. Matter Mater. Phys.*, 2008, **77**, 115123.
50 G. H. Zou, C. S. Lin, H. Jo, G. Nam, T. S. You and K. M. Ok, *Angew. Chem., Int. Ed.*, 2016, **128**, 12257–12261.
51 X. H. Dong, L. Huang, C. F. Hu, H. M. Zeng, Z. E. Lin, X. Wang, K. M. Ok and G. H. Zou, *Angew. Chem., Int. Ed.*, 2019, **58**, 6528–6534.

